EXAMINATION OF PHYLLOSILICATE-BEARING MATERIALS IN THE VICINITY OF THE NILI FOSSAE USING THERMAL INFRARED DATA. M. L. McDowell[1] and V. E. Hamilton[1], [1]Hawai'i Institute of Geophysics and Planetology, University of Hawai'i, 1680 East-West Rd, Honolulu, HI 96822 (mcdowell@hawaii.edu).

Introduction: The visible to near-infrared (VNIR) spectrometer Observatoire pour la Mineralogie, l'Eau, les Glaces et l'Activité (OMEGA) onboard the Mars Express spacecraft has identified the presence of phyllosilicates, specifically clay minerals, in some places on the Martian surface [e.g. 1-4]. These detections in the VNIR provide an opportunity to study the spectral character of confirmed Martian phyllosilicate-bearing materials in the thermal infrared (TIR) range.

Phyllosilicates are identified in VNIR data by reflectance minima at ~1.4, 1.9, and 2.2 – 2.4 μm from O-H, H-O-H, and metal-OH bonds in the minerals. In TIR data (Si, Al)-O bonds result in the most prominent features [e.g. 5]. In some cases the TIR features of phyllosilicates are broad with low spectral contrast, which may make their identification at low abundances more difficult than for other minerals with stronger, more narrow features (e.g. olivine [6]). Because mineral spectra are assumed to add linearly in proportion to their abundance in the TIR wavelength region (shown to be a good approximation in most cases [e.g. 7, 8]), a mixed spectrum can be linearly deconvolved to determine the modeled mineral abundances. Linear deconvolutions of Martian surface spectra collected by TES report phyllosilicate abundances of ~15% over much of the surface [e.g. 9, 10]. The reliability of such abundances have been debated because of the possibility that they maybe not be distinguished from silica or poorly crystalline phases [5, 10], or because they may be surface coatings of phyllosilicate material which would not add linearly and result in an exaggerated abundance [9]. OMEGA VNIR detections of phyllosilicate-bearing material appear to be more limited on the Martian surface than these TES TIR modeled abundances would suggest. A more detailed study of the phyllosilicate-bearing areas may be helpful in understanding the characteristics of phyllosilicates in TIR data and reliable TES detection limits for modeled abundances. We analyze TIR data for qualitative and quantitative spectral characteristics that may be used to differentiate phyllosilicate-bearing material from non-phyllosilicate-bearing material.

Study area. One of the few notable concentrations of phyllosilicate detections by OMEGA is in the region in and surrounding the Nili Fossae [2, 3], the concentric grabens along the northwest margin of the Isidis basin. In our investigation we look at four of the occurrences of phyllosilicate-bearing material (suggested to be Fe- and Mg-rich clays such as nontronite [2]) in this region. The location of these study areas is shown in Figure 1. The 'trough' study area has been proposed as a landing site for the Mars Science Laboratory [11]. *Michalski et al.* [12] have previously reported an initial TIR investigation of the 'basement outcrop' in this region. Their study suggests that subtle compositional differences may be present, but that the materials are dominantly basaltic.

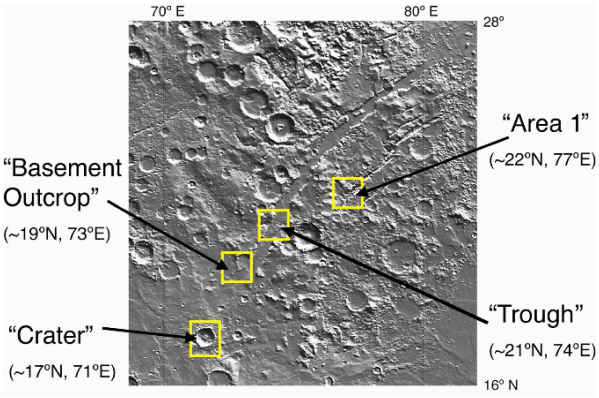

FIGURE 1: Shaded relief map of the region around the Nili Fossae indicating the four areas analyzed in this work.

Approach: We use multiple data sets and methods to conduct a detailed analysis of our study areas in the vicinity of the Nili Fossae. TIR data for this work is from the Thermal Emission Imaging System (THEMIS) and the Thermal Emission Spectrometer (TES). THEMIS is a multispectral TIR spectrometer with a visible imaging subsystem onboard Mars Odyssey [13], and TES is a hyperspectral TIR spectrometer included on the Mars Global Surveyor spacecraft [14].

To investigate spectral variation in the study areas, we perform a decorrelation stretch (DCS) [15] on THEMIS daytime TIR images. This stretch uses three specified wavelength bands and redefines each axis in the way that maximizes variation and removes correlated information between bands. We produce atmospherically corrected THEMIS spectra by removing the atmospheric components of each image using the process described by *Bandfield et al.* [16].

We select the best quality TES spectra available for the area of interest and ratio them with spectra of the surrounding region from the same orbit to determine if any difference is apparent in these measured spectra [17]. We conduct linear deconvolutions [7] of the TES spectra and analyze the resulting modeled abundances.

We also use factor analysis and target transformation, as described in [18], to help retrieve independently-varying spectral shapes in the region, an approach that does not rely on the exact spectral shape to be present in a pre-determined end-member set.

Additionally, we are in the process of using numerical mixtures of basalt and phyllosilicates to better understand the detection limits and uncertainty of modeled phyllosilicate abundances. We combine a basalt spectrum (e.g., Mars' surface type 1 –ST1) with that of a phyllosilicate (e.g., nontronite) in increasing proportions from 0 to 100%. We then deconvolve the resulting spectra and compare the modeled phyllosilicate abundances to the known proportion of the phyllosilicate spectrum in the mixture. We will vary this approach by using a range of phyllosilicates, along with basalt spectra produced by different methods (i.e., ST1, a lab-measured basalt spectrum, and a spectrum synthesized from a combination of the lab spectra of basaltic mineral components). In addition, we will investigate the effect on the modeled abundances of other variables such as noise, spectral resolution, wavelength range, and the absence of the phyllosilicate in the mixture from the end-member set. This work is similar to that of *Koeppen and Hamilton* [19], who used simple numerical mixtures to analyze uncertainties of phyllosilicates and glasses as part of their larger work of phyllosilicate and glass discrimination. Our study builds on this by using complex mixtures that more accurately represent TES measurements of the Martian surface. We are concerned primarily with phyllosilicate abundances, though we are also aware of the anti-correlation that may exist between phyllosilicate and glass abundances [19], which will be examined in our study. *Koeppen and Hamilton* [19] also showed the importance of including multiple phyllosilicate and glass phases in end-member sets. In the future we will perform laboratory studies of physical mixtures of phyllosilicates and basalt.

Results: Figure 2 shows the DCS radiance images of the four study areas (THEMIS bands 9/7/5 as R/G/B). Spectral variation is expressed as differences in color in the DCS images. The phyllosilicate-bearing materials clearly exhibit differences in color from the surrounding basaltic materials. The blue boxes in each image indicate the area within the phyllosilicate-bearing material from which atmospherically corrected emissivity spectra were averaged to produce the spectra in Figure 3. The red boxes in the DCS images indicate the area from which the "plains" emissivity spectra are derived (this area is outside of the image for the Crater study area). We include additional spectra from interesting areas of spectral variation for the Area 1 study region. The shape of the THEMIS spectra from

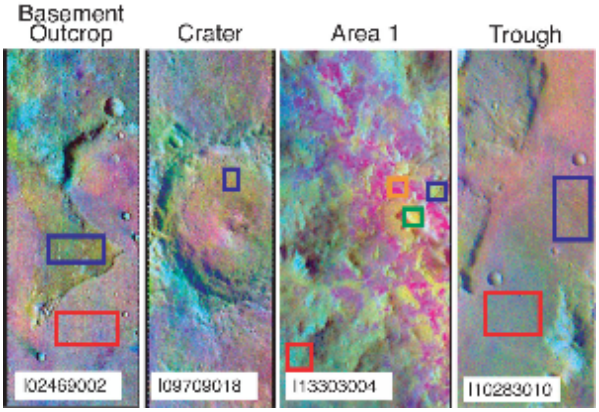

FIGURE 2: DCS radiance images of the four study areas (THEMIS bands 9/7/5 in R/G/B). Colored boxes correspond to the average spectra in Figure 3.

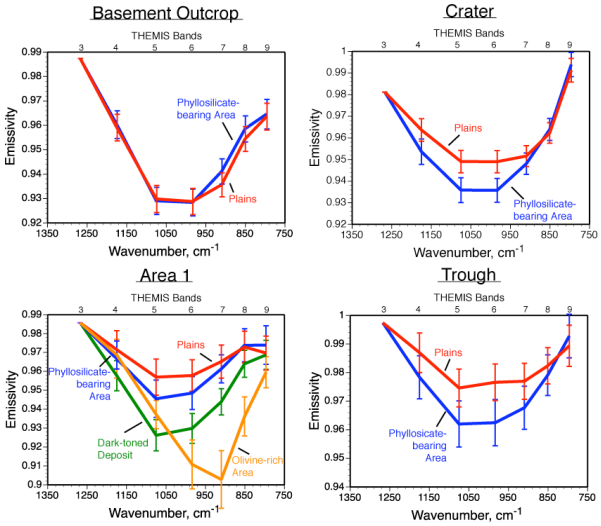

FIGURE 3: THEMIS atmospherically corrected emissivity spectra from each of the four study areas. Specific locations from which spectra are derived are indicated by the boxes in Figure 2.

the phyllosilicate-bearing materials differs from that of the non-phyllosilicate-bearing materials. Error bars on the emissivity spectra represent the standard deviation of the averaged spectra.

Ratios of TES spectra from the regions of interest to their surrounding plains do show small differences, likely a result of differing compositions. However, these ratio spectra do not appear to be strongly similar to the spectra of phyllosilicates from the kaolinite, illite, and smectite classes (including nontronite).

Atmosphere-removed TES spectra, shown in Figure 4, differ in shape between the phyllosilicate-bearing area and the surrounding plains, though these differences are slight in some cases, such as for the Basement Outcrop study area. The modeled abundances of these surface spectra are shown in Figure 4.

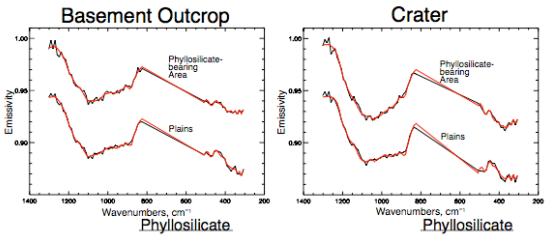

Basement Outcrop	Phyllosilicate Area	Plains
Plagioclase Feldspar	21	22
Pyroxene	31	30
Olivine	3	5
Phyllosilicates	23	19
K-rich Glass	8	8
Other	14	16

Crater	Phyllosilicate Area	Plains
Plagioclase Feldspar	37	28
Pyroxene	20	33
Olivine	6	8
Phyllosilicates	15	13
K-rich Glass	14	6
Other	9	12

Area 1	Phyllosilicate Area	Plains
Plagioclase Feldspar	10	19
Pyroxene	36	32
Olivine	30	12
Phyllosilicates	9	19
K-rich Glass	2	0
Other	12	18

Trough	Phyllosilicate Area	Plains
Plagioclase Feldspar	26	21
Pyroxene	30	26
Olivine	10	6
Phyllosilicates	11	21
K-rich Glass	13	11
Other	10	16

FIGURE 4: TES atmosphere-removed surface emissivity spectra for each phyllosilicate-bearing area and the surroundings. Black lines are measured spectra and red lines are the best-fit modeled spectra. Plains spectra are offset by –0.05. Below each graph are the modeled abundances (%). The 'other' category consists of phases modeled well below the detection limit.

Detection limits and uncertainties are generally thought to be ~10-15% [20]. Comparisons of the modeled abundances further suggest that the phyllosilicate-bearing materials and the plains are different in overall composition. However, the modeled phyllosilicate abundances show either little variation between the region of interest and the plains (e.g., for the Basement Outcrop and the Crater study areas), or have the opposite trend than would be expected (i.e., have a higher phyllosilicate abundance for the plains than the region of interest). Additionally, many of these modeled abundances are near or below the general detection limit of 10-15%. The Area 1 spectra are dominated by olivine, which is a result of sub pixel mixing between the small phyllosilicate-bearing spots and adjacent olivine-rich material.

We are currently analyzing the results from factor analysis and target transformation of TES data. Though we have identified unique spectral shapes, we have not yet found any indication that phyllosilicates are varying independently of the surrounding material.

Initial numerical mixture analysis results with mixtures of the ST1 and nontronite spectra suggest that phyllosilicates as a group may be overestimated in modeled abundances by up to ~10% when using our "control" values for variables in the deconvolution (i.e. no added noise, 1302-305 cm^{-1} range, TES resolution, specific nontronite end-member present in end-member set) (Figure 5). We observe this same behavior when the range over which the spectra are deconvolved is decreased to 350 cm^{-1} and 400 cm^{-1}. The modeled abundance of nontronite alone is also overestimated in these trials by up to ~6, 13, and 17% for the three wavelength ranges from 1302 to 305, 350, and 400 cm^{-1}, respectively. We show this first case in Figure 5. However, modeled abundances remain at zero unless the proportion of nontronite in the mixture is above ~15-20%. Work on these numerical mixture analyses is ongoing.

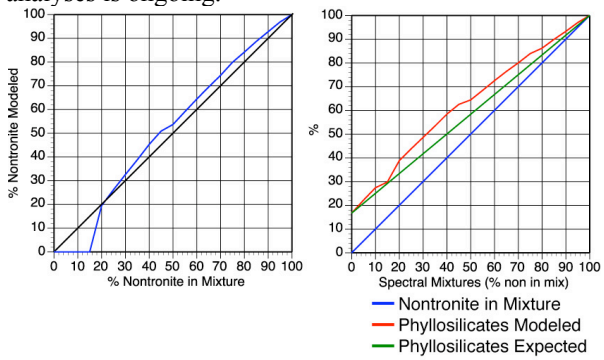

FIGURE 5: Left - Plot comparing the % nontronite modeled to the proportion of nontronite in the numerical mixture for our 'control' study (see text for details). Right - Plot illustrating the % phyllosilicates (as a group) modeled (red) compared to the % of phyllosilicates expected (green). Expected values are calculated from the % nontronite in the mixture with the addition of the phyllosilicates modeled for ST1 in proportion to the % ST1 in the mixture.

Discussion: In an effort to understand the qualitative behavior that might be expected when phyllosilicates are with mixed basaltic material within the same THEMIS pixel, we produce numerical mixtures of ST1 and nontronite at THEMIS resolution in proportions between 0 and 100% (Figure 6). As the proportion of nontronite in the mixture increases, THEMIS bands 5 and 6 decrease in emissivity whereas bands 4 and 7 increase, resulting in an increase in slope between bands 6 and 7 (Figure 6). A comparison of the THEMIS spectra for the regions of interest and the plains shows that they display slope differences between bands 6 and 7, with the spectra of the phyllosilicate-bearing materials having the higher slope (Figure 7). This is consistent with, but not necessarily solely

attributable to, an increase in phyllosilicate abundance in the regions of interest.

TES spectral shapes and their modeled abundances are clearly different between the regions of interest and the plains, but the differences between these regions represent more than just the presence or absence of phyllosilicates. There are other changes that reflect either different starting materials, chemical alteration, the addition of younger materials, or all of the above. The lack of a resemblance of spectral ratios to phyllosilicate shapes also suggests a difference in overall composition not specifically related to the phyllosilicates. This does not preclude the presence of phyllosilicates in these areas, but our results may indicate that they are not in high enough abundances to be reliably detected by TES. Our further investigations into detections limits for phyllosilicates may help to better constrain these abundances.

Summary & Ongoing Work: We observe spectral differences between the locations where OMEGA detects phyllosilicates and the surrounding materials in the vicinity of the Nili Fossae. In THEMIS data the spectral characteristics are consistent with an increase in phyllosilicate abundance in the regions of interest, though other interpretations may be possible. TES data indicate compositional differences between the regions of interest and the plains, but a change in phyllosilicate abundance is not distinguishable. This may be a result of low absolute phyllosilicate abundance, which may allow for detection by OMEGA but limits reliable detection with TES TIR data. We are continuing to investigate the implications of the modeled abundances from the numerical mixture analyses and the effects of varying the basalt and phyllosilicate used, along with other deconvolution constraints. Future laboratory analysis of physical basalt and phyllosilicate mixtures may provide additional insight into the detection limits and uncertainties of phyllosilicates in TES data.

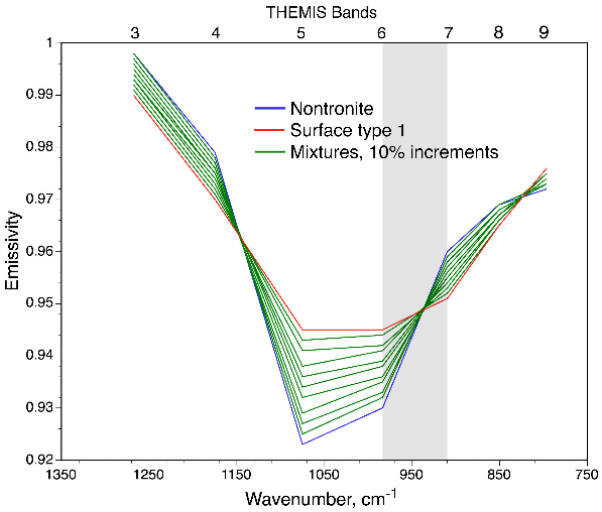

FIGURE 6: Numerical mixtures of nontronite and ST1 at THEMIS resolution. The shadowed area highlights the change in slope between bands 6 & 7.

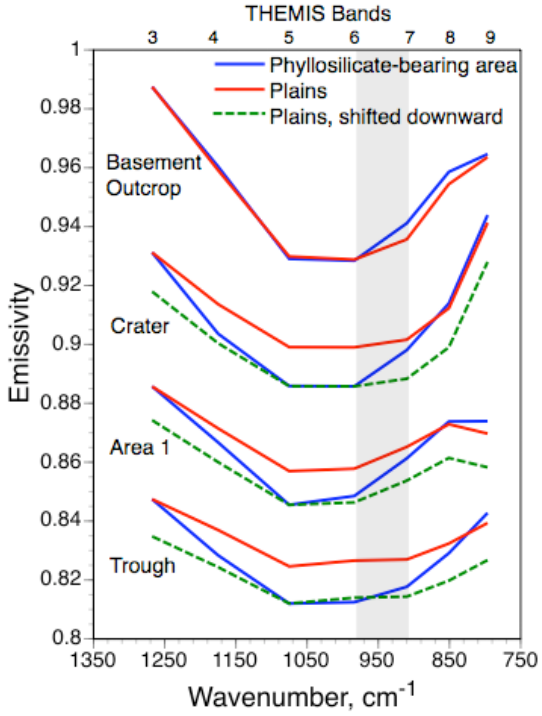

FIGURE 7: THEMIS atmospherically corrected spectra. Each spectral group is offset by –0.05 from the previous group. Where needed the plains spectrum is shifted downward to better illustrate differences in slope between the plains and the phyllosilicate-bearing spectra.

References: [1] Bibring J-P. et al. (2005) *Science, 307*, 1576-1581. [2] Poulet F. et al. (2005) *Nature, 438*, 623-627. [3] Poulet F. et al. (2006) LPSC XXXVII, Abst. #1698. [4] Mustard J. F. et al. (2006) LPSC XXXVII, Abst. #1683. [5] Michalski J. R. et al. (2006) *JGR, 111*, doi:10.1029/2005JE002438. [6] Hamilton V. E. et al. (2003) *M&PS, 38*, 871-886. [7] Ramsey and Christensen (1998) *JGR, 103*, 577-596. [8] Feely and Christensen (1999) *JGR, 104*, 24195-24210. [9] Bandfield J. L. et al. (2000) *Science, 287*, 1626-1630. [10] Wyatt and McSween (2002), *Nature, 417*, 263-266. [11] Mustard J. F. et al. (2006) First MSL Landing Site Workshop. [12] Michalski J. R. et al. (2006) LPSC XXXVII, Abst. #1242. [13] Christensen P. R. et al. (2004) *SSR, 110*, 85-130. [14] Christensen P. R. et al. (2001) *JGR, 106*, 23823-23871. [15] Gillespie A. R. et al. (1986) *Rem. Sens. Env., 20*, 209-235. [16] Bandfield J. L. et al. (2004) *JGR, 109*, doi:10.1029/2004JE002289. [17] Ruff and Christensen (2002) *JGR, 107*, 5127. [18] Bandfield J. L. et al. (2000) *JGR, 105*, 9573-9587. [19] Koeppen and Hamilton (2005) *JGR, 110*, doi:10.1029/2005JE002474 [20] Christensen P. R. et al. (2000) *JGR, 105*, 9609-9621.